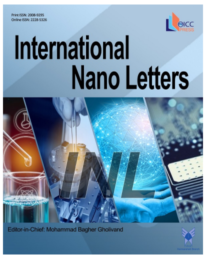

Volume 15, Issue 4, 152514 (1-8)

International Nano Letters (INL)

https://doi.org/10.57647/inl.2025.1504.14

Structural Tuning of ZnO Nanorods via Seed-Layer Engineering for High Speed n-ZnO/p-Si UV Photodetector

Samaneh Jabbarivand[1], Moahammad Hossein Majles Ara[1,*], Soraya Muosavi[1,2], Ali Kazempour[1]

[1] *Nanophysics Lab, Faculty of Physics, Kharazmi University, Tehran, Iran.*
[2] *Department of Physics, Faculty of Physics and Chemistry, Alzahra University, Tehran, Iran.*

[*] **Corresponding author:** majlesara@khu.ac.ir

Original Research

Received:
5 August 2025
Revised:
10 November 2025
Accepted:
27 November 2025
Published online:
30 December 2025

Abstract:
The effect of seed layer thickness on the optical and electrical properties of ZnO nanorods (NRs) for fast-response UV photodetector applications was investigated. Vertically aligned ZnO NRs were grown via a hydrothermal method using seed layers with various thicknesses ranging from 350 nm to 550 nm. FESEM characterization revealed that the synthesized ZnO NRs had average diameters of 71 – 175 nm and lengths of 1.3 – 2 µm. UV-Vis spectra indicated that the sample with the thinnest seed layer (350 nm), which exhibited a higher aspect ratio, showed enhanced absorption in the UV region. p-n heterojunction photodetectors (PDs) based on the synthesized ZnO NRs were fabricated, and their I-V and I-t characteristics were evaluated. The results demonstrated that optimizing the seed layer thickness in accordance with the UV wavelength significantly improves the photodetector's responsivity, sensitivity, and quantum efficiency, while also achieving remarkably fast response and recovery times. These findings highlight the critical role of structural tuning in enabling high-performance, fast-response UV photodetectors.

Keywords: ZnO nanorods; Seed layer tuning; Fast-response UV photodetector; PN photodiode

Cite this article: Jabbarivand, S., Majles Ara, M.H., Muosavi, S., Kazempour, A.Structural Tuning of ZnO Nanorods via Seed-Layer Engineering for High Speed n-ZnO/p-Si UV Photodetector. *Int. Nano Lett.* **15**(4), 152514 (2025).

1. Introduction

In the photonics century, photodetectors underpin lots of technologies of modern life. These devices are applicable in an extended range of fields. Among these devices, ultraviolet (UV) photodetectors have attracted particular interest due to their potential for high-performance applications, where fast response, high quantum efficiency, and low noise are essential [1, 2]. Modern nanoscale semiconductor photodetectors are crucial building blocks of today's optical systems [3]. Zinc oxide (ZnO) nanostructure is known as a low-cost nontoxic intrinsic n-type semiconductor material with a direct wide band gap (3.37 eV) and a large exciton binding energy (60 meV) at room temperature, which transmits visible light [4, 5]. These unique properties make ZnO especially suitable for UV detection, and its significant optical and electronic characteristics have introduced promising features for opto-electrical devices such as light-emitting diodes, solar cells, gas sensors, and photodiodes [6–8]. Among different photodetector structures, P-N junction photodiodes (P-N PDs) are an attractive choice due to their simplicity of fabrication. The P-N structure is particularly advantageous because it combines fast response with high responsivity and low signal-to-noise ratio, which are crucial for UV photodetector performance [9, 10]. The performance of UV PDs highly depends on the structure of the active area, which is responsible for absorption of the incident light, carrier generation, and transport, ultimately producing the electrical output signal [11]. One-dimensional nanostructures such as nanorods and nanowires have demonstrated high sensitivity in UV PD applications due to the increase in aspect ratio, the presence of deep-level defects that enhance carrier lifetime, and reduction of structural disorders [12, 13]. Several methods have been utilized to grow 1-D ZnO nanostructures, including chemical bath deposition, hydrothermal synthesis, and others [2, 14, 15]. Among these, the hydrothermal method is particularly suitable for fabricating vertically aligned ZnO nanorods (NRs) due to its simplicity, low cost, low-temperature process, energy efficiency, and capability for large-scale production on diverse substrates [16]. Modifying different factors such as precursor concentration, pH, growth time, and temperature allows control and optimization of the nanorods' morphology. Different substrates are used to grow ZnO NRs, and among them, P-type Si is convenient [2]. Furthermore, the surface of the substrate directly affects the size of the nanorods. Using a seed layer is crucial to reduce lattice mismatch between the rod and the substrate, and the morphology and thickness of the seed layer strongly influence optical absorption, alignment, and electronic behavior of the nanorods, which are key for enhancing UV photodetector performance [17, 18].

In this study, we systematically investigate how the thickness of the ZnO seed layer affects the structural, optical, and electrical properties of ZnO nanorods and their performance in n-ZnO/p-Si UV photodetectors. We have demonstrated that aspect ratio tuning via seed-layer thickness is a tool to actively tailor a performance trade-off; high-aspect-ratio structures maximize responsivity at shorter wavelengths, while an optimized intermediate ratio enhances internal carrier efficiency, leading to superior responsivity and faster response at near-band-edge wavelengths. This aspect-ratio-dependent spectral tuning offers a clear design principle for wavelength-selective photodetectors using a simple, solution-based process. For this purpose, three different thicknesses of the ZnO seed layer are prepared on the p-type Si wafer as a substrate. ZnO NRs are then grown by hydrothermal method under constant growth conditions. Comprehensive characterization techniques are employed to analyze the morphology, structure, and optical response of the nanorods. The results indicate that the lowest thickness sample has higher efficiency due to nanorods with greater aspect ratio and higher capability for UV light absorption. P-N photodiodes are fabricated based on each type of ZnO NRs to study their electrical properties and UV responsivity. Overall, our findings demonstrate that optimizing the seed layer thickness is an effective strategy to achieve fast, high-responsivity UV photodetectors with enhanced performance [1, 19].

2. Experimental details

2.1 Materials

Zinc acetate dihydrate, $Zn(CH_3CO_2)_2 \cdot 2H_2O$ (99%, Merck), absolute ethanol (99.9%, Merck) as a solvent, Triethylamine (TEA) (99%, Merck), Zinc nitrate hexahydrate $Zn(NO_3)_2 \cdot 6H_2O$ (99%, Merck), and Hexamethylenetetramine (HMTA) (99%, Merck) were used as precursors. ZnO nanorods (NRs) were synthesized in two separate steps: (1) preparation of a uniform layer of ZnO as a seed layer and (2) growth of the ZnO NRs by hydrothermal method [20, 21].

2.2 ZnO NRs synthesis

P-type (100) Si substrates were used for seed layer deposition and the growth of ZnO NRs. The substrates were cleaned using standard RCA-1 and RCA-2 procedures to remove organic residues, rinsed in DI water, and dried. Zinc acetate dihydrate was dissolved in a mixture of absolute ethanol and TEA to achieve a 1 M ZnO solution, with a molar ratio of zinc acetate to TEA of 5:2. The solution was stirred for 30 min at room temperature to obtain a homogeneous transparent stable solution. The ZnO solution was then spin-coated on the Si substrates under three different conditions to achieve the desired seed layer thicknesses. Subsequently, the samples were heated in an electric oven at 90 °C for 1 h and annealed at 400 °C for 2 h [20].

For the growth of ZnO NRs, zinc nitrate hexahydrate and HMTA (molar ratio 1:1) were dissolved in DI water to prepare a 1 M ZnO solution. The annealed seed layers were immersed in this solution inside an autoclave, which was then placed in an oven at 90 °C for 8 h. After cooling to room temperature, the samples were washed with DI water, and the annealing process was completed by heating at 400 °C for 2 h [21].

2.3 P-N heterojunction fabrication

Ohmic contacts were implemented to fabricate the P-N heterojunction samples for electrical measurements. An Ag wire was attached to the surface of the grown NRs using Ag paste. The HF solution was used to etch part of the grown NR surface to allow attachment of the second Ag wire to the Si substrate, completing the P-N heterojunction structure [20, 21].

3. Results

3.1 Structural and morphological characterization

SEM analysis was used to study the structure and morphological properties of the grown ZnO NRs on different thicknesses of the seed layers. According to Fig. 1, it is clear that the thickness of the initial seed layer remarkably affects the diameter and length of the grown ZnO NRs. As can be seen, lower thickness results in lower diameter as well as longer length. The lower diameter comes from the smaller grains which are formed in the lower thicknesses [22, 23]. The specifications of the seed layers and NRs can be found in Table 1. Besides the effects of seed layer thickness on the shape of ZnO NRs, SEM images clearly demonstrate the wurtzite structure of ZnO NRs, which confirms the high quality of the synthesis. Depending on the application requirements, the length and diameter of the rods can be adjusted as well.

The Atomic Force Microscopy (AFM) was applied to investigate the initial roughness of the seed layers prior to the growth process (Fig. 2). The root mean square (RMS) roughness values of the different thicknesses, as well as the bare silicon wafer, are listed in Table 2. There is a direct correlation between the seed layer thickness and the resulting surface roughness, such that increasing the thickness leads to higher RMS values [23]. The observed roughness

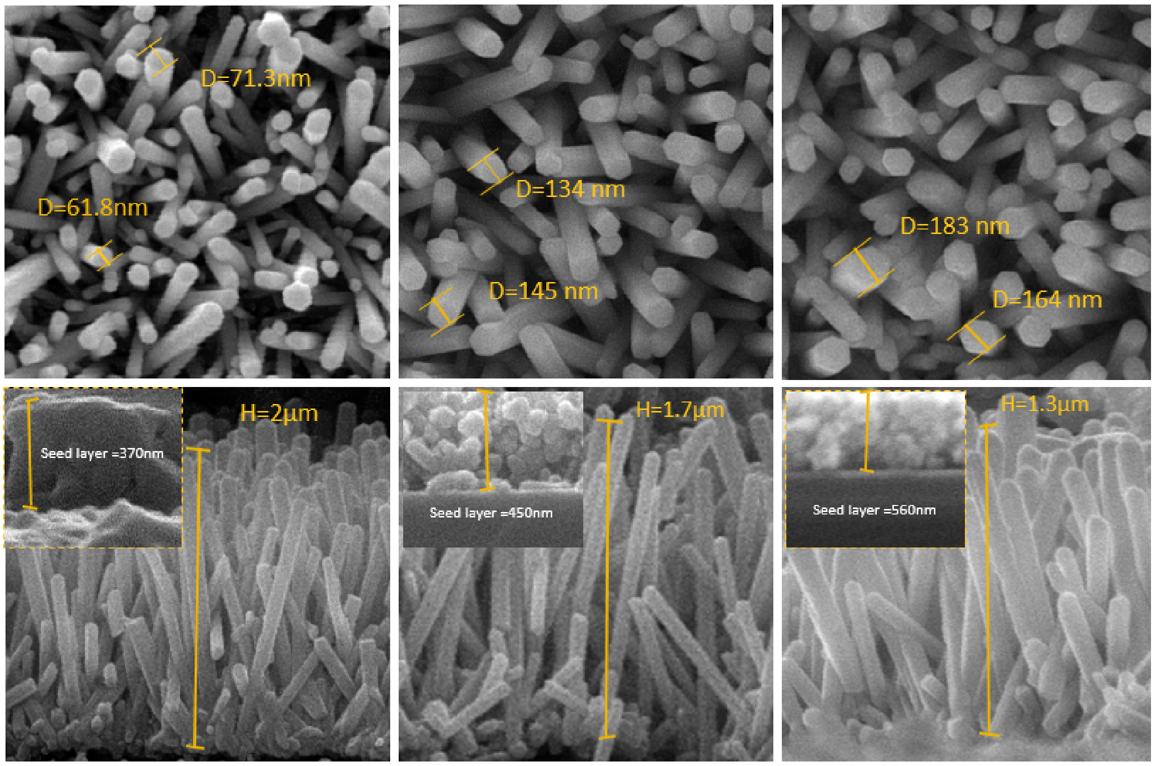

Figure 1. The top view and cross section images of ZnO NRs on different seed layers (S1, S2, S3).

Table 1. The structure properties of ZnO NRs.

Seed layer's thickness (in average)	NR's diameter (in average)	NR's length (in average)
S1 = 370 nm	70 nm	2 μm
S2 = 450 nm	140 nm	1.7 μm
S3 = 560 nm	175 nm	1.3 μm

enhancement is mainly attributed to the formation of larger grains accompanied by a reduction in grain density [22]. SEM micrographs further support this trend by illustrating how variations in RMS roughness affect the morphology of the ZnO nanorods. Lower seed layer thickness results in ZnO NRs with greater lengths and smaller diameters, consistent with improved nucleation uniformity on smoother surfaces [22, 23]. In addition, roughness plays a vital role in determining the conductivity of the resulting structures. A decrease in surface roughness reduces carrier trapping sites and consequently enhances conductivity due to the higher carrier mobility [22]. The reported RMS roughness values are derived from measurements on representative, uniform areas of each sample. While these values provide a clear comparison of morphological changes by the seed layer, a full statistical error analysis was not specified for these specific measurements.

3.2 Optical characterization

Figure 3 depicts the UV-Visible absorption spectra of the samples. Comparing the spectra reveals that all samples have a peak in the UV region (between 350 and 380 nm). Based on recent studies, reducing the seed layer thickness enhances the aspect ratio of the grown nanorods (NRs), which in turn increases the UV absorption [24, 25]. According to the observed rising trend of absorption in the UV region, the sample with the higher aspect ratio exhibits stronger absorption. The increase in UV absorption is attributed to the longer NRs, higher aspect ratio, and larger photoactive area. Therefore, the seed layer with 350 nm initial thickness exhibits more UV light absorption compared to other samples due to the longer NRs with smaller diameters [24]. Furthermore, a slight blue shift is observable with the increment of aspect ratio (AR) of the NRs.

It is evident that the energy band gaps of the NRs change as a function of their aspect ratios, resulting in different absorption wavelengths. Figure 4 plots $(\alpha h\nu)^2$ versus energy bandgap for all samples. The energy band gap for each sample is determined by the intercept of the linear extrapolation of the graph on the band gap energy axis [24]. The relation of parameters appears in equation (1):

$$(\alpha h\nu)^2 = h\nu - E_g \tag{1}$$

where α is absorption coefficient, h is Planck's constant, ν is frequency, and E_g is energy band gap. Also, α is calculated by the following equation:

$$\alpha = \frac{1}{d} \times \ln(\frac{1}{T}) \tag{2}$$

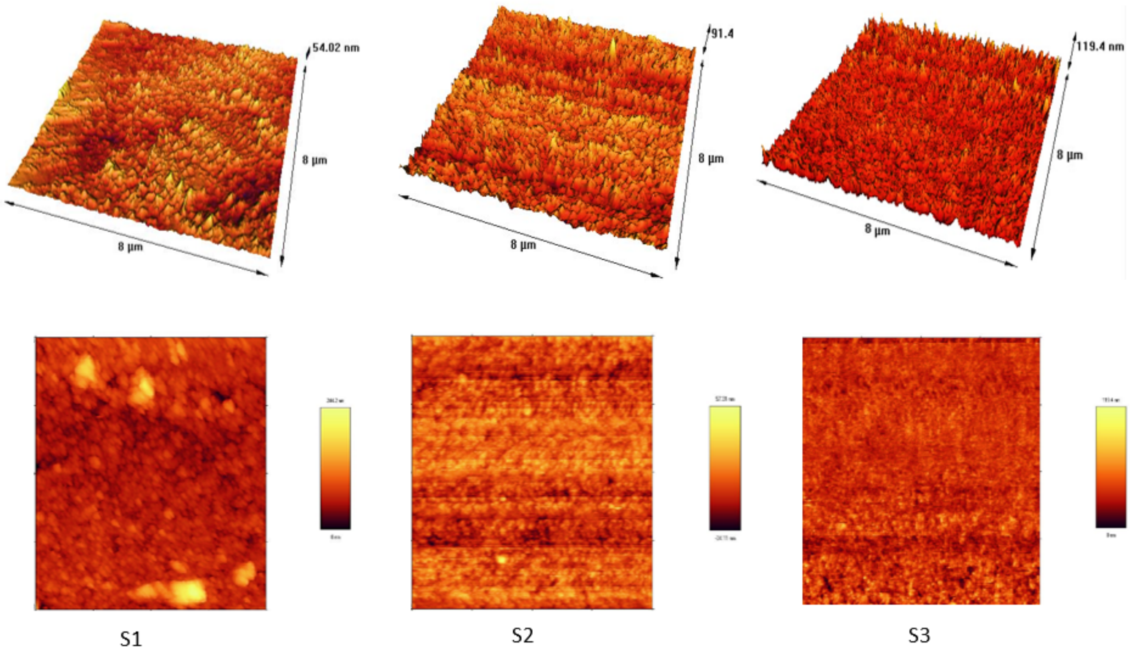

Figure 2. AFM images determined roughness of different seed layers with various thickness (S1, S2, S3).

Table 2. The average surface roughness of different samples before ZnO NRs growth.

Sample	RMS roughness (nm)
Sample 1 = 350 nm	2.88
Sample 2 = 450 nm	5.88
Sample 3 = 560 nm	8

where d is the sample thickness, and T is the transmittance. The band gap energy is obtained for each sample using the Tauc plot [24]. Considering the Tauc plots in Fig. 4, the band gap energy of S1 is higher than that of the other samples, and it decreases as the seed layer thickness increases [24, 25]. The band gaps of S1, S2, and S3 were determined to be approximately 3.22 eV, 3.20 eV, and 3.19 eV, respectively. As the thickness of the seed layer reduces, the grain sizes diminish, and the diameter of the NRs decreased. On the contrary, an increase in the diameter of the NRs, leading to a smaller band gap [24]. In addition, ZnO NRs exhibit a lower band gap energy compared to bulk ZnO (3.36 eV), which is related to the optical confinement effect of nanostructure formation [24].

3.3 Electro-optical characterizations

Current-voltage (I-V) and current-time (I-t) curves were plotted to evaluate the performance characteristics of the fab-

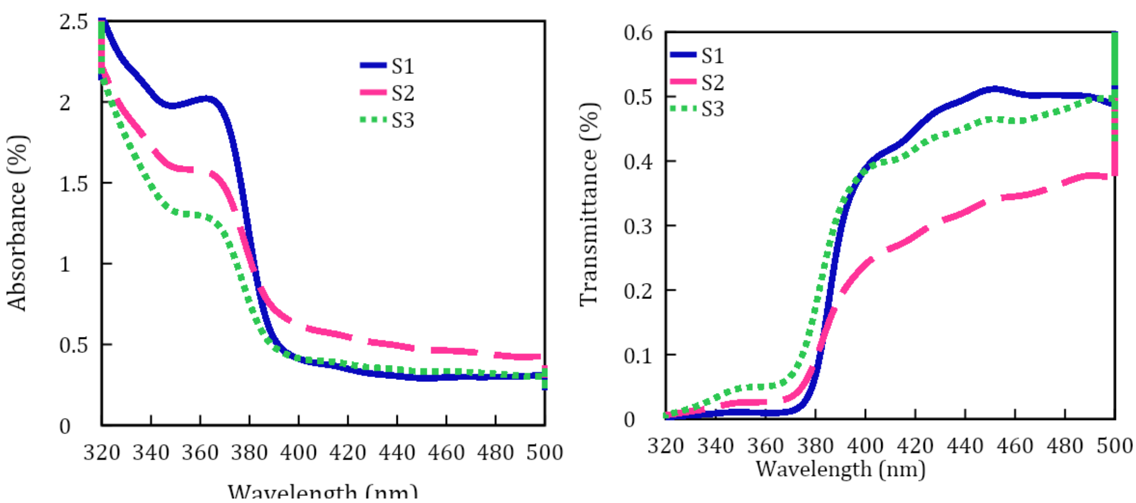

Figure 3. UV absorption and transmittance of different ZnO NRs samples.

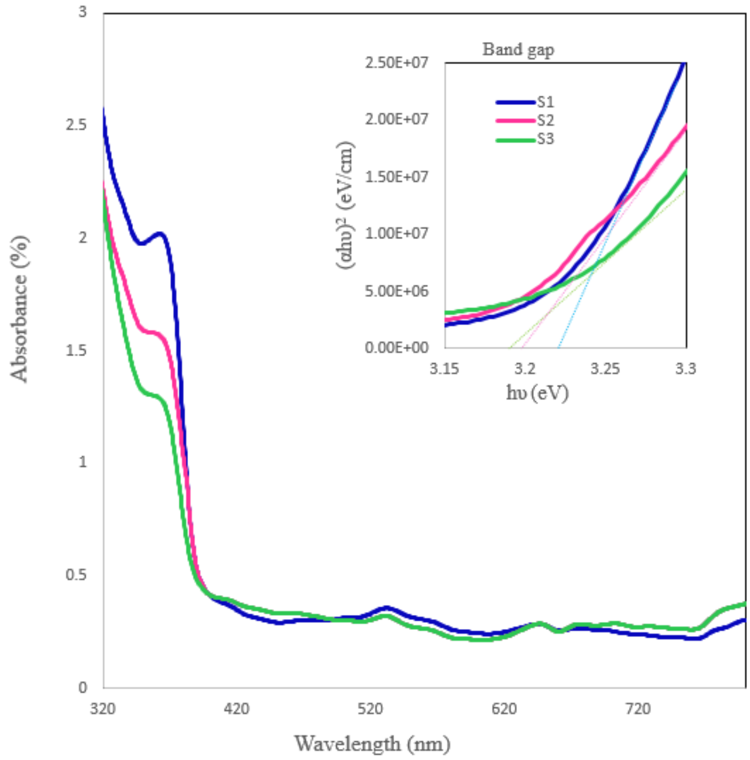

Figure 4. Variations of $(\alpha h\nu)^2$ versus energy bandgap for various samples.

ricated photodiodes based on ZnO NRs with different aspect ratios. Previous studies indicate that ZnO nanorod-based photodetectors typically exhibit their highest responsivity in the 350 – 400 nm wavelength range due to dominant near-band-edge absorption [26, 27]. Therefore, the samples were illuminated under UV light (500 mW) at three critical wavelengths of 365 nm, 380 nm, and 395 nm. Table 3 summarizes the extracted parameters, including responsivity, specific detectivity, quantum efficiency (QE), response time, and recovery time. The illumination was on the acrive area which was fabricated ZnO nanostructure in dimension of (0.5 cm × 0.5 cm).

The responsivity (R) and specific detectivity (D^*) of the device can be calculated by the following equations:

$$R = \frac{I_{ph}}{P_{inc}} \tag{3}$$

$$D^* = R\left(\frac{P_{inc}}{2eI_{dark}}\right)^{1/2} \tag{4}$$

where I_{ph} (A) is the photocurrent of the device, and P_{inc} (W) is the optical power of incident light [2, 4, 23].

Quantum efficiency (QE) is another expressed factor of the device which can be evaluated by equation (3) as follows:

$$QE = \frac{Rhc}{\lambda e} = 1240\frac{R}{\lambda} \times 100 \tag{5}$$

where R (A/W) is the responsivity of the device, h is the Plank constant, c is the speed of light, λ (nm) is the wavelength and e is the electron. Based on Fig. 5, a reduction in aspect ratio leads to a noticeable decrease in dark current. The maximum dark current was recorded for S1 ($\sim$ 3.52 µA), while the minimum was obtained for S3 ($\sim$ 0.3 µA). This trend indicates that samples with higher AR exhibit a larger density of free carriers and stronger internal electric field separation, consistent with prior reports [28].In contrast, the photocurrent behavior follows a different trend. The photocurrent strongly depends on wavelength, with the maximum response occurring near the band-gap region of each sample. For S1, S2, and S3, maximum photocurrents were 19.07 µA at 365 nm, 2.9 µA at 380 nm, and 1.36 µA at 395 nm, respectively. The photocurrent of S1 decreases significantly with increasing wavelength, whereas S3 exhibits relatively higher photocurrents at longer wavelengths. Furthermore, the device with the highest AR (S1)

Table 3. Different parameters of ZnO NRs samples based on UV PD devices.

Wavelength	$\lambda = 365$ nm				$\lambda = 380$ nm				$\lambda = 395$ nm			
Parameters	Responsivity (A/W)	Sensitivity (%)	QE (%)	Detectivity (Jones)	Responsivity (A/W)	Sensitivity (%)	QE (%)	Detectivity (Jones)	Responsivity (A/W)	Sensitivity (%)	QE (%)	Detectivity (Jones)
S1	0.4	103	135	$1.5*10^9$	0.21	27	111	$1.3*10^9$	0.002	72	5.3	$0.6*10^9$
S2	0.04	57	14	$0.2*10^9$	0.04	60	20	$0.35*10^9$	0.03	60	20	$0.34*10^9$
S3	0.025	84	8.5	$0.3*10^9$	0.01	126	25	$1.1*10^9$	0.01	161	25	$1.17*10^9$

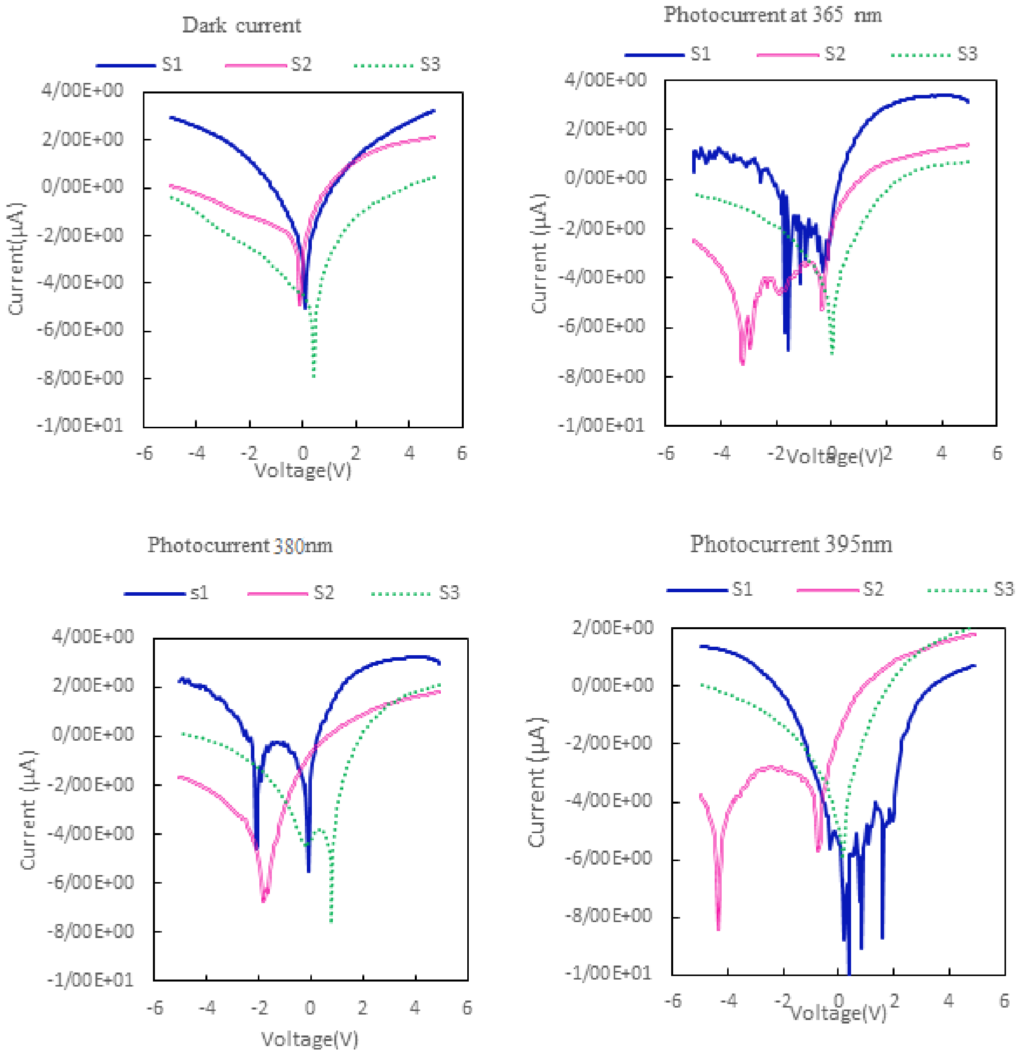

Figure 5. I-V curves of different samples at various wavelengths under dark and illumination conditions.

exhibits the greatest responsivity. A higher aspect ratio increases photon path length, enhances light trapping, and strengthens inter-rod scattering leading to increased carrier generation. Efficient light trapping occurs when the AR enables effective multi-angle scattering, refraction, and reflection, thereby increasing optical absorption [29, 30].

Light-scattering efficiency also depends strongly on wavelength and decreases exponentially with increasing wavelength, which aligns with the observed reduction in responsivity at longer wavelengths [31]. S1 has the lowest seed layer thickness, resulting in smaller NR diameters and longer NR lengths, which produce a higher AR. This structural configuration induces a slight blue shift in the absorption edge, thereby improving absorption at shorter wavelengths, consistent with modern experimental findings [32]. Accordingly, S1 demonstrated the highest responsivity at 365 nm. This value decreased gradually toward 395 nm due to reduced photon absorption and limited generation of electron–hole pairs.

In contrast, S3 showed higher responsivity at longer wavelengths (particularly 395 nm). This behavior originates from the red-shifted band-gap edge of S3, causing its maximum absorption to occur closer to 395 nm, which results in higher photocurrent and responsivity at that wavelength [33]. Therefore, tuning the seed-layer thickness effectively adjusts the ZnO NR morphology and enables optimized responsivity, detectivity, and quantum efficiency across targeted UV wavelengths.

Figure 6 illustrates the I–t behavior of the device at various wavelengths for two consecutive cycles. All measurements were performed at an applied voltage of 2 V, with illumination and dark intervals of 15 seconds. Upon UV exposure, the current increased rapidly until reaching a saturation level, whereas the current decreased immediately when the device returned to dark conditions. Table 4 summarizes the response and recovery times at different wavelengths. To more clearly highlight the temporal performance of the photodetectors, the results indicate a rapid and efficient current transition under UV illumination. Accordingly, S1 exhibits the shortest response and recovery times at $\lambda = 365$ nm, while S3 demonstrates superior temporal performance at $\lambda = 395$ nm due to its faster rise and decay characteristics. Absorption increases with increasing aspect ratio (AR), primarily due to enhanced optical scattering and improved

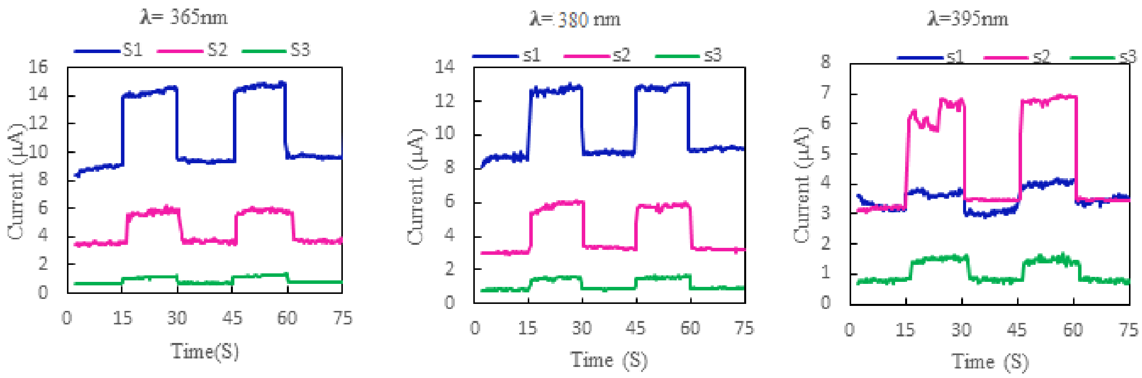

Figure 6. The I-t response of ZnO NRs PD for different samples at bias voltage of 2 V.

Table 4. Response and recovery times of different ZnO NRs samples based on UV PD devices.

	UV = 365 nm		UV = 380 nm		UV = 395 nm	
	Rise time (s)	Fall time (s)	Rise time (s)	Fall time (s)	Rise time (s)	Fall time (s)
S1	0.063	0.34	0.07	0.37	0.2	0.48
S2	0.1	0.73	0.06	0.31	0.2	0.3
S3	0.1	0.73	0.2	0.43	0.1	0.3

light-trapping effects, which significantly intensify photocarrier generation and reduce device resistance [34].
For each device, the fastest photocurrent transition occurs at wavelengths corresponding to the strongest optical absorption, typically near the band-gap region of the ZnO nanorods. Thus, the minimum response time for each sample appears close to its band-edge absorption wavelength, consistent with the fundamental carrier dynamics governed by nanorod geometry and defect-mediated recombination pathways. These rapid rise and decay characteristics further confirm the strong temporal efficiency of the ZnO NR-based photodetectors developed in this work. The obtained response and recovery times align well with previously reported high-performance ZnO NR photodetectors, demonstrating competitive temporal performance metrics [35, 36].

4. Conclusion

The optimization of ZnO nanorod (NR) structures for UV photodetector applications was successfully achieved by systematically studying the effect of seed layer thickness on the optical and electrical properties of the ZnO NRs. The sample with the thinnest seed layer (350 nm) produced longer nanorods with smaller diameters and higher aspect ratios, which led to enhanced UV light absorption, particularly in the 370 – 380 nm wavelength range. Electrical characterization through I-V measurements under dark and illuminated conditions confirmed improved photocurrent generation for the optimized samples. Time-resolved I-t analysis at 365, 375, and 395 nm revealed that the sample with the thinnest seed layer (S1) exhibited faster response and recovery times, higher responsivity, quantum efficiency, and sensitivity at 365 nm, whereas S3 demonstrated superior performance at 395 nm.
These observations indicate a clear correlation between nanorod aspect ratio and photodetector response speed: higher aspect ratio nanorods facilitate more efficient carrier transport along the rod axis, reducing carrier recombination and thereby improving both response and recovery times. Therefore, UV photodetector performance can be finely tuned for specific wavelengths by selecting an appropriate ZnO NR sample with optimized seed layer thickness, guided by bandgap considerations and structural aspect ratio. Overall, this study demonstrates that structural engineering of ZnO nanorods via seed layer optimization is a viable strategy for achieving fast-response, wavelength-specific, high-performance UV photodetectors suitable for practical optoelectronic applications.

Authors Contribution
All authors contributed equally to the conception, design, execution, and writing of this work. All authors read and approved the final manuscript.

Availability of data and materials
The data that support the findings of this study are available from the corresponding author, upon reasonable request.

Conflict of interests
The authors declare that they have no known competing financial interests or personal relationships that could have appeared to influence the work reported in this paper.

References

[1] Y. Zhang et al. High-performance UV photodetectors based on ZnO nanostructures. *ACS Applied Electronic Materials*, (2023). DOI: https://doi.org/10.1021/acsaelm.2c01431.

[2] F. Li et al. Ultraviolet photodetectors: Progress and challenges. *Materials Today: Proceedings*, (2023). DOI: https://doi.org/10.1016/S0254-0584(23)00228-6.

[3] J. Kumar et al. Recent advances in nanoscale photodetectors. *Optical Materials*, (2021). DOI: https://doi.org/10.1016/j.optmat.2021.111057.

[4] L. Wang et al. ZnO nanostructures for optoelectronic applications. *Optical and Quantum Electronics*, (2020). DOI: https://doi.org/10.1007/s11082-020-02329-1.

[5] H. Chen et al. ZnO nanostructures for UV sensors. *Management Insight*, (2022). DOI: https://doi.org/10.1108/MI-03-2022-0046.

[6] R. Singh et al. ZnO-based light-emitting devices. *IEEE Access*, (2021). DOI: https://doi.org/10.1109/ACCESS.9320483.

[7] T. Patel et al. Gas sensors based on ZnO nanorods. *Optical Materials*, (2021). DOI: https://doi.org/10.1016/j.optmat.2021.111018.

[8] M. Zhao et al. ZnO photodiodes for UV detection. *Materials Science in Semiconductor Processing*, (2020). DOI: https://doi.org/10.1016/j.mssp.2020.105359.

[9] P. Kumar et al. P-N junction UV photodiodes. *Sensors and Actuators A*, (2020). DOI: https://doi.org/10.1016/j.sna.2020.112547.

[10] S. Wang et al. High-speed UV photodetectors. *Journal of Physics D: Applied Physics*, (2023). DOI: https://doi.org/10.1088/1361-6528/acbf59.

[11] H. Li et al. Carrier transport in ZnO nanorods. *Journal of Physics: Conference Series*, (2024). DOI: https://doi.org/10.1088/1742-6596/2624/1/012007.

[12] A. Singh et al. 1D ZnO nanostructures for photodetector applications. *MRS Energy & Sustainability*, (2023). DOI: https://doi.org/10.1557/s43578-023-00941-x.

[13] Y. Liu et al. Nanorod-based UV sensors. *Sensors and Actuators B*, (2025). DOI: https://doi.org/10.1016/j.snb.2024.128455.

[14] F. Li et al. Hydrothermal growth of ZnO nanorods. *Materials Science in Semiconductor Processing*, (2022). DOI: https://doi.org/10.1016/j.mssp.2022.106748.

[15] K. Zhang et al. Chemical bath deposition of ZnO nanorods. *Optik*, (2022). DOI: https://doi.org/10.1016/j.ijleo.2022.168273.

[16] R. Kumar et al. Hydrothermal synthesis of ZnO nanorods for photodetection. *Applied Surface Science*, (2023). DOI: https://doi.org/10.1016/j.apsusc.2023.161498.

[17] S. Gupta et al. Effect of seed layer thickness on ZnO nanorods. *Materials Science and Engineering A*, (2022). DOI: https://doi.org/10.1016/j.msea.2022.112345.

[18] L. Wang et al. Morphology control in ZnO nanorods. *Journal of Alloys and Compounds*, (2022). DOI: https://doi.org/10.1016/j.jallcom.2022.163256.

[19] H. Zhao et al. Optimizing seed layer thickness for high-performance UV photodetectors. *Solar Energy Materials & Solar Cells*, (2025). DOI: https://doi.org/10.1016/j.solmat.2024.115678.

[20] R. Rouzbahani, Ara M.H. Majles, B. Efafi, and S.S. Mousavi. A comprehensive optimization of aluminum concentration in ZnO nanocrystals by novel simple methods. *Electronic Materials Letters*, pages 931–937, (2015).

[21] R. Wang et al. Functionalized ZnO@TiO_2 nanorod array film loaded with $ZnIn_{0.25}Cu_{0.02}S_{1.395}$: Synthesis, characterization and enhanced visible light driven water splitting. *Nanoscale*, pages 11082–11092.

[22] Tolosa M.D. Reyes et al. Influence of seed layer thickness on properties of electrodeposited ZnO nanostructured films. *SN Applied Sciences*, (2019). DOI: https://doi.org/10.1007/s42452-019-1293-7.

[23] G. Yergaliuly et al. Effect of thickness and reaction media on properties of ZnO thin films by SILAR. *Scientific Reports*, (2022). DOI: https://doi.org/10.1038/s41598-022-04782-2.

[24] Y. Gu et al. Quantum confinement in ZnO nanorods. *Applied Physics Letters*, pages 3833–3835, (2004).

[25] X. Wang et al. Seed layer thickness effect on ZnO nanorods for UV absorption enhancement. . *Scientific Reports*, (2024). DOI: https://doi.org/10.1038/s41598-024-73352-5.

[26] J. Li et al. High-performance ZnO nanorod UV photodetectors under near-band-edge excitation. *IEEE Transactions on Electron Devices*, (2015). DOI: https://doi.org/10.1109/TED.2015.2436355.

[27] S. Mohapatra et al. UV photodetection enhancement in ZnO nanostructures. *Materials Today: Proceedings*, (2022). DOI: https://doi.org/10.1016/j.matpr.2021.12.410.

[28] H. Zhang et al. Carrier transport and dark current mechanisms in ZnO nanostructures. *Scientific Reports*, (2025). DOI: https://doi.org/10.1038/s41598-025-21149-5.

[29] A. Shankar et al. Light trapping and optical absorption enhancement in ZnO nanorod arrays. *Journal of Materials Science*, (2020). DOI: https://doi.org/10.1007/s10853-020-05618-y.

[30] L. Chen et al. Optical scattering and absorption modulation in semiconductor nanostructures. *Nanotechnology*, (2019). DOI: https://doi.org/10.1088/1361-6528/ab0ee5.

[31] S. Roy et al. Wavelength-dependent scattering effects in ZnO nanostructures. *Applied Surface Science*, (2017). DOI: https://doi.org/10.1016/j.apsusc.2017.03.115.

[32] M. Zhao et al. Bandgap engineering and excitonic effects in high-aspect-ratio ZnO nanorods. *Journal of the Optical Society of America B*, (2023). DOI: https://doi.org/10.1364/JOSAB.488207.

[33] R. Ferreira et al. Wavelength-selective responsivity tuning in ZnO nanorod photodetectors. *Materials Research Bulletin*, (2022). DOI: https://doi.org/10.1016/j.materresbull.2021.111036.

[34] M. Uddin et al. Enhanced UV absorption and light-trapping in high-aspect-ratio ZnO nanostructures. *New Journal of Chemistry*, (2021). DOI: https://doi.org/10.1039/D1NJ04382J.

[35] S.R. Jadwisienczak et al. High-responsivity ZnO nanostructure UV photodetectors with optimized carrier dynamics. *Materials Science and Engineering B*, (2023). DOI: https://doi.org/10.1016/j.mseb.2023.116411.

[36] A.K. Singh et al. Self-powered UV photodetectors based on ZnO nanostructures: Fast response and enhanced transport mechanisms. *AIP Advances*, (2021). DOI: https://doi.org/10.1063/5.0038521.